Hydrogen Bonding Networks and Solid-state Conversions in Benzamidinium Salts

Naghmeh Kamali, Marwah Aljohani, Patrick McArdle* and Andrea Erxleben*

School of Chemistry, National University of Ireland, Galway, Ireland

ABSTRACT

Ten benzamidinium salts of carboxylic acids, amides and sulfonamides have been crystallized from solution. Single-crystal X-ray analyses revealed various hydrogen bonding motifs which are discussed in terms of supramolecular synthons and graph sets. Benzamidinium hydrogen maleate (**5a**) crystallizes as large needles of up to > 3 cm length. Attempts to influence the crystal habit and size through a change of solvent and the presence of additives yielded a second polymorph (**5b**). The formation of the benzamidinium salts by mechanochemical reaction was also investigated. Grinding of benzamidine with nicotinic acid, salicylic acid, *p*-aminobenzoic acid, cyanuric acid, pimelic acid, saccharin and sulfathiazole with mortar and pestle or using a ball-mill gave compounds identical to those obtained by crystallization from solution. Time-dependent X-ray powder patterns of a stoichiometric benzamidine/cyanuric acid mixture suggested that the mechanochemical salt formation occured *via* the amorphous state. Ball-milling of benzamidine with sulfamerazine generated amorphous benzamidinium sulfamerazinate that was stable towards crystallization for at least two weeks, when stored at 25 % relative humidity.

1. INTRODUCTION

The amidine functional group ($RC(=NH)NH_2$) is an important pharmacophore that is present in a large number of drugs and pharmaceuticals. Amidines display a variety of pharmacological activities and have applications as antibacterial and antifungal drugs (*e. g.* propamidine, dibromopropamidine), antimicrobial (*e. g.* hexamidine, pentamidine), antiparasitic, antibiotic (*e. g.* amdinocillin), antiviral (*e. g.* taribavirin, ribavirin), anti-inflammatory, cardiovascular, anti-diabetic, central nervous system and antineoplastic drugs.[1-7] Due to the similarity of the amidine group to the guanidine group of L-arginine, amidines can interact with the L-arginine binding site of NO synthase.[8] Several benzamidine derivatives are potent competitive inhibitors of trypsin- and trypsin-like enzymes and serineproteases.[9,10] Furthermore, amidines can act as thrombin and topoisomerase inhibitors[9,10] and as antagonists of the P2X7 and M1 muscarimic receptor.[11] Sugar amidines have been investigated as inhibitors of carbohydrate-processing enzymes.[12-23]

Amidines are strong bases and are usually protonated under physiological conditions. Various amidines are formulated as salts such as alkylsulfonates. The positively charged amidinium group has four protons that can form strong charge-assisted hydrogen bonds to the counterion. Here we report the crystal structures of a range of benzamidinium salts of carboxylic acids, amides and sulfonamides. In all cases, extensive H bonding interactions give rise to 1D, 2D or 3D supramolecular structures.

Furthermore, we have studied the mechanochemical synthesis of crystalline benzamidinium salts. Mechanochemistry has recently been recognized as an attractive alternative to the traditional solution crystallization method.[24] The mechanochemical preparation of salts - either by manual grinding with a mortar and pestle or in a mixer mill - offers various advantages such as the inherent 'green' nature and ease of experimental design.[25,26] As a modification of neat grinding, solvent-drop or liquid-assisted grinding, *i.e.* grinding in the presence of sub-stoichiometric amounts of solvent, can be applied as a screening tool for salt formation and new crystal forms.[27]

2. MATERIALS AND METHODS

Benzamidine, nicotinic acid, salicylic acid, *p*-aminobenzoic acid, maleic acid, malonic acid, pimelic acid, cyanuric acid, saccharin, sulfathiazole, and sulfamerazine were purchased from Sigma Aldrich. Commercial sulfathiazole and sulfamerazine were polymorphs form III and I, respectively, as confirmed by X-ray powder diffraction. Solvents were of analytical or spectroscopic grade, purchased from commercial sources and used without further purification.

Preparation of Single Crystals of 1 – 10. 50 mg (0.42 mmol) benzamidine was dissolved in 2 mL H_2O (**1**, **4**, **5a**), methanol (**6**-**10**), acetone (**2**) or isopropanol (**3**). A solution of 0.42 mmol of the respective carboxylic acid, amide or sulfonamide in 2 mL of the same solvent was added and the mixture was left to stand at room temperature to allow for slow evaporation of the solvent. Colourless crystals appeared within a few days.

Preparation of Single Crystals of 5b. 20 μL pyridine-2-carboxaldehyde or picolylamine was added to a solution of 50 mg (0.42 mmol) benzamidine and 50 mg (0.43 mmol) maleic acid in 4 mL ethanol. Large cubes of **5b** crystallized after 3 days alongside needles of **5a**.

Solid-state and Solvent-drop Grinding. Method A. Benzamidine (300 mg, 2.5 mmol) and 1 equivalent of the respective carboxylic acid, amide or sulfonamide were placed in a mortar and the mixture was ground manually for 5 minutes.

Method B. Benzamidine (300 mg, 2.5 mmol) and 1 equivalent of the respective carboxylic acid, amide or sulfonamide were placed in a mortar. After addition of one drop of solvent, the mixture was ground manually for 2 minutes. Then another drop of solvent was added and grinding was continued for another 3 minutes.

Method C. Benzamidine and 1 equivalent of the respective carboxylic acid, amide or sulfonamide (600 mg in total) were combined with or without the addition of 50 μL solvent. The mixtures were ground for 20 minutes in an oscillatory ball mill (Mixer Mill MM400, Retsch GmbH & Co., Germany) at 25 Hz using a 25 cm^3 stainless steel grinding jar and one 12

mm stainless steel ball. Any small amount of solvent present was allowed to evaporate and the resulting material was characterized by X-ray powder diffraction.

Instrumentation. FT-IR spectra were recorded on a PerkinElmer FT-IR spectrometer fitted with an ATR accessory. DSC experiments were performed on a STA625 thermal analyzer from Rheometric Scientific. The heating rate was kept constant at 10 °C min^{-1} unless stated otherwise and all runs were carried out from 25 °C to 250 °C. The measurements were made in open aluminum crucibles, nitrogen was used as the purge gas in ambient mode, and calibration was performed using an indium standard.

X-ray Powder Diffraction. X-ray powder patterns of samples obtained by grinding or crystallization from solution were recorded on an Inel Equinox 3000 powder diffractometer between 5 and 90 ° (2θ) using Cu K_α radiation (λ = 1.54178 Å, 35 kV, 25 mA). Theoretical powder patterns for **1**-**10** were calculated using the Oscail software package.[28]

Crystal Structure Determination and Refinement. Crystal data for **1**-**10** were collected at room temperature on an Agilent (formerly OxfordDiffraction) Xcalibur CCD diffractometer using graphite-monochromated Mo-K_α radiation (λ= 0.71069 Å).[29] The structures were solved by direct methods and subsequent Fourier syntheses and refined by full-matrix least squares on F^2 using using SHELXS-97 and SHELXL-97[30,31] within the Oscail package.[28] The scattering factors were those given in the SHELXL program. Hydrogen atoms were located in the difference Fourier maps and refined isotropically (**1**, **2**, **4**, **5a**, **5b**, **7**-**10**) or generated geometrically and refined as riding atoms with isotropic displacement factors equivalent to 1.2 times those of the atom to which they were attached (**3**, **6**). Graphics were produced with ORTEX.[28] Crystallographic data and details of refinement are reported in Tables 1 and 2.

Supplementary crystallographic data have been deposited with the Cambridge Crystallographic Data Centre, CCDC no. 1031758 (**1**), 1031757 (**2**), 1031756 (**3**), 1031755 (**4**), 1031753 (**5a**), 1031754 (**5b**), 1031752 (**6**), 1031750 (**7**), 1031749 (**8**), 1031748 (**9**), 1031747 (**10**). Copies of the data may be obtained free of charge from The Director, CCDC, 12 Union

Road, Cambridge CB2 1EZ, UK (fax:+44-1223-336033; e-mail: deposit@ccdc.cam.ac.uk or www: http://www.ccdc.cam.ac.uk).

Table 1. Crystallographic Data for Compounds 1 - 5

	1	**2**	**3**	**4**	**5a**	**5b**
Formula	$C_{13}H_{13}N_3O_2$	$C_{14}H_{14}N_2O_3$	$C_{14}H_{15}N_3O_4$	$C_{10}H_{12}N_2O_4$	$C_{33}H_{36}N_6O_{12}$	$C_{11}H_{12}N_2O_4$
M_r	243.26	258.27	257.29	224.22	708.68	236.23
Crystal habit	block	plate	block	block	needle	cube
Crystal size (mm)	0.30 x 0.30 x 0.20	0.50 x 0.35 x 0.15	0.25 x 0.20 x 0.15	0.20 x 0.20 x 0.10	0.60 x 0.10 x 0.05	0.40 x 0.30 x 0.30
Crystal system	monoclinic	monoclinic	monoclinic	triclinc	triclinic	monoclinic
Space group	$P2_1$	$P2_1/c$	$P2_1/c$	P-1	P-1	$P2_1/n$
Unit cell dimensions						
a [Å]	9.5379(12)	7.3446(4)	19.367(3)	5.5336(5)	11.4553(7)	8.8197(6)
b [Å]	5.7387(7)	16.385(1)	7.1978(8)	8.9229(9)	11.5940(8)	21.1800(12)
c [Å]	12.5211(18)	11.1975(7)	19.4919(16)	10.9447(11)	14.6223(10)	12.3153(10)
α [°]				87.095(8)	68.150(6)	
β [°]	109.146(15)	105.157(6)	104.881(11)	89.016(8)	76.810(6)	93.492(7)
γ [°]				75.137(8)	74.391(6)	
V [Å^3]	647.44(15)	1300.65(14)	2626.0(6)	521.65(9)	1718.1(2)	2296.2(3)
Z	2	4	4	2	2	8
D_{calc} (g cm^{-3})	1.248	1.319	1.302	1.427	1.370	1.367
μ(Mo Kα) (cm^{-1})	0.087	0.094	0.090	0.112	0.106	0.106
F(000)	256	544	1088	236	744	992
2θ range (°)	6.6 - 52.6	6.5 - 54.2	6.0 - 50.4	7.5 - 52.7	5.9 - 52.7	5.9 - 52.7
No. measd. reflections	2766	9842	17796	3452	11963	9356
No. unique reflections (R_{int})	2043 (3.1 %)	2841 (2.3%)	4788 (7.7%)	2121 (2.2 %)	7027 (2.3%)	4688 (3.8%)
No. observed reflections	1015 ($I > 2\sigma(I)$)	2108 ($I > 2\sigma(I)$)	2713 ($I > 2\sigma(I)$)	1406 ($I > 2\sigma(I)$)	4040 ($I > 2\sigma(I)$)	2643 ($I > 2\sigma(I)$)
No. parameters	274	228	403	182	604	403
Final R_1, wR_2	R_1 = 5.3%,	R_1 = 4.6%,	R_1 = 10.6%,	R_1 = 5.2%,	R_1 = 5.0%,	R_1 = 5.7%,
(observed reflections) [a]	wR_2 = 9.4%	wR_2 = 10.9%	wR_2 = 28.6%	wR_2 = 11.6%	wR_2 = 9.1%	wR_2 = 10.7%
Goodness-of-fit (observed reflections)	0.945	1.018	1.054	1.024	1.002	1.021

[a] $R_1 = \Sigma| |F_o| - |F_c| | / \Sigma|F_o|$; $wR_2 = [\Sigma w(F_o^2 - F_c^2)^2 / \Sigma w(F_o^2)^2]^{1/2}$; $w^{-1} = \sigma^2(F_o^2) + (aP)^2$; $P = (F_o^2 + 2F_c^2)/3$.

Table 2. Crystallographic Data for Compounds 6 - 10

	6	**7**	**8**	**9**	**10**
Formula	$C_{21}H_{28}N_4O_4$	$C_{16}H_{17}N_5O_2S_2$	$C_{18}H_{20}N_6O_2S$	$C_{14}H_{13}N_3O_3S$	$C_{10}H_{13}N_5O_4$
M_r	400.47	375.47	384.46	303.33	267.25
Crystal habit	needle	plate	needle	block	needle
Crystal size (mm)	0.30 x 0.10 x 0.10	0.30 x 0.20 x 0.15	0.60 x 0.20 x 0.08	0.60 x 0.45 x 0.45	0.60 x 0.15 x 0.10
Crystal system	orthorhombic	monoclinic	orthorhombic	monoclinic	monoclinic
Space group	$P2_12_12_1$	$P2_1/c$	Pbca	$P2_1$	P2/c
Unit cell dimensions					
a [Å]	5.6600(4)	13.9493(9)	14.0370(8)	10.9623(8)	12.1599(15)
b [Å]	18.8049(16)	8.3273(4)	16.2988(6)	5.8715(3)	7.1495(11)
c [Å]	19.4650(13)	16.9440(9)	16.6980(7)	12.0212(9)	13.5183(14)
α					
β [°]		113.288(7)		116.754(9)	90.035(10)
γ					
V [Å^3]	2071.8(3)	1807.9(2)	3820.3(3)	690.91(8)	1175.2(3)
Z	4	4	8	2	2
D_{calc} (g cm^{-3})	1.284	1.370	1.337	1.458	1.460
μ(Mo Kα) (cm^{-1})	0.090	0.315	0.196	0.248	0.06
F(000)	856	784	1616	316	280
2θ range (°)	6.0 - 54.2	5.9 - 52.7	6.2 - 50.0	6.8 - 52.7	6.0 - 50.6
No. measd. reflections	6393	7722	10042	2873	7240
No. unique reflections (R_{int})	4132 (2.0%)	3699 (2.8 %)	3361 (4.9 %)	1985 (2.5 %)	2156 (4.0 %)
No. observed reflections	2393 ($I > 2\sigma(I)$)	2695 ($I > 2\sigma(I)$)	2094 ($I > 2\sigma(I)$)	1882 ($I > 2\sigma(I)$)	1654 ($I > 2\sigma(I)$)
No. parameters	262	295	312	242	180
Final R_1, wR_2	R_1 = 4.3%,	R_1 = 4.3%,	R_1 = 5.8%,	R_1 = 2.6%,	R_1 = 4.5%,
(observed reflections) [a]	wR_2 = 7.2%	wR_2 = 10.7%	wR_2 = 11.8%	wR_2 = 6.6%	wR_2 = 11.0%
Goodness-of-fit (observed reflections)	0.929	1.004	1.053	1.058	1.016

[a] $R_1 = \Sigma||F_o| - |F_c|| / \Sigma|F_o|$; $wR_2 = [\Sigma w(F_o^2 - F_c^2)^2 / \Sigma w(F_o^2)^2]^{1/2}$; $w^{-1} = \sigma^2(F_o^2) + (aP)^2$; $P = (F_o^2 + 2F_c^2)/3$.

3. RESULTS

X-ray Structures. X-ray suitable crystals of the following benzamidinium salts were obtained by slow evaporation of alcoholic or aqueous solutions of 1:1 mixtures of benzamidine and the respective carboxylic acid, sulfonamide or amide; $bzamH^+nic^-$ (**1**), $bzamH^+sal^-$ (**2**), $bzamH^+pab^-$ (**3**), $bzamH^+malo^-$ (**4**), $bzamH^+male^-$ (**5a, 5b**), $(bzamH^+)_2pim^{2-}$ (**6**), $bzamH^+stz^-$ (**7**), $bzamH^+smz^-$ (**8**), $bzamH^+sac^-$ (**9**), and $bzamH^+cya^-$ (**10**) ($bzamH^+$ = benzamidinium, nic^- = nicotinate, sal^- = salicylate, pab^- = *p*-aminobenzoate, $malo^-$ = malonate, $male^-$ = maleate, pim^{2-} = pimelate, stz^- = sulfathiazolate, smz^- = sulfamerazinate, sac^- = saccharinate, cya^- = cyanurate). A variety of hydrogen bonding motifs was observed which will be discussed in terms of supramolecular synthons and graph sets. The geometric parameters of the hydrogen bonding interactions are listed in Table S1 (Supporting Information).

H Bonding Motifs in Benzamidinium Carboxylates. The $R_2^2(8)$ homodimer is a very common supramolecular motif in carboxylic acids, amides and amidines and as expected, $R_2^2(8)$ rings resulting from pairs of charge-assisted N-H···O hydrogen bonds between the benzamidinium cation and carboxylate anion are found in all benzamidinium carboxylates. Furthermore, $R_2^1(6)$, $R_4^4(12)$, and $R_4^2(8)$ rings consisting of two carboxylate anions and two benzamidinium cations, $R_6^4(16)$ rings built up by three carboxylate and three benzamidinium groups and $R_8^6(24)$ rings containing four carboxylate and four benzamidinium groups are observed (Scheme 1).

Figure 1 shows the hydrogen bonding motif in $bzamH^+nic^-$ (**1**). Ion pairs with the $R_2^2(8)$ motif are linked into undulated sheets with $R_6^4(16)$ rings being present between the $R_2^2(8)$ synthons. Neighbouring sheets are connected through C-H···N hydrogen bonds between C5-H5 of the benzamidinium aromatic ring and the pyridine nitrogen of nicotinate (N3···C5 = 3.474(8) Å).

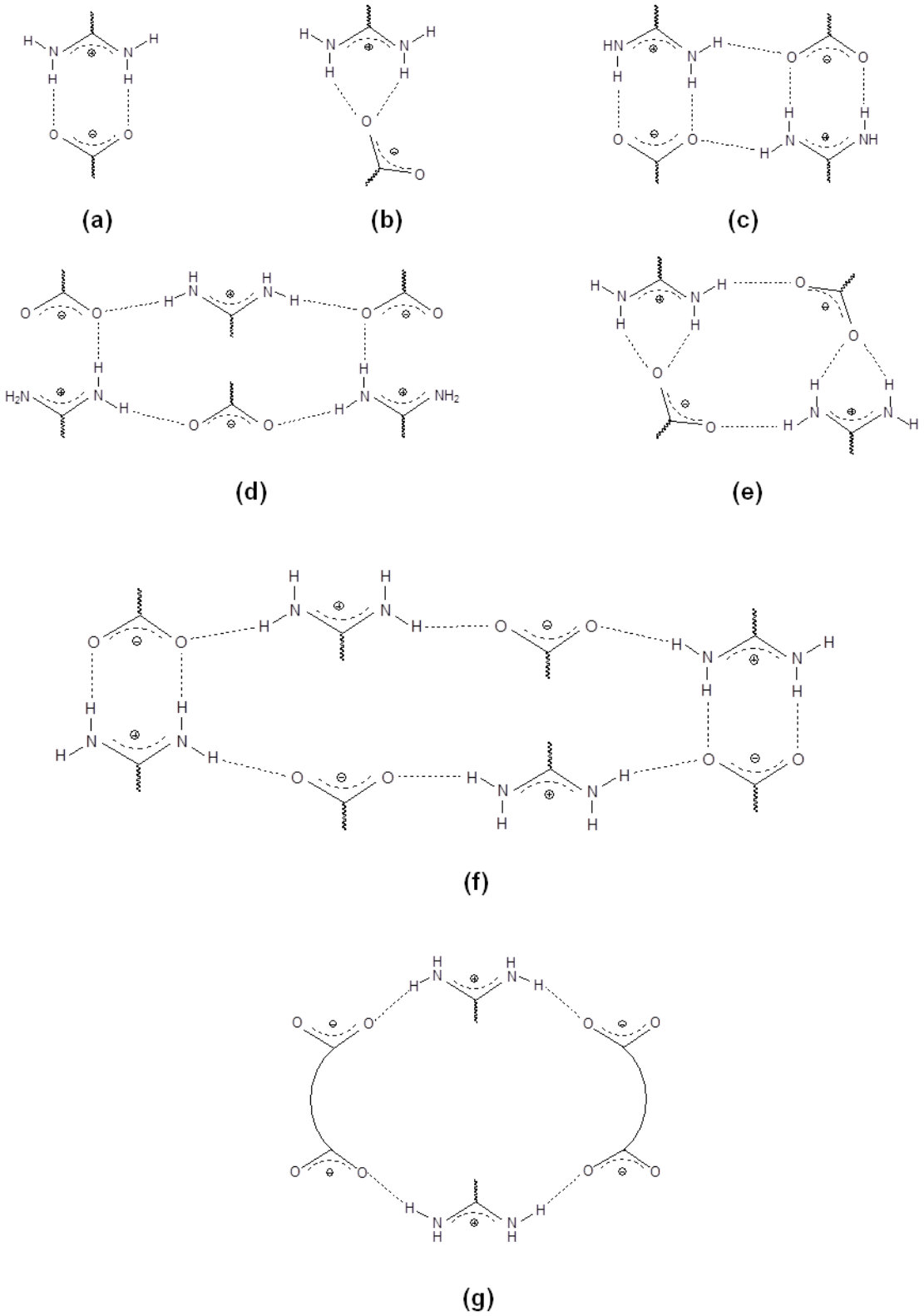

Scheme 1. Hydrogen bonding motifs in benzamidinium carboxylates. (a) $R_2^2(8)$, (b) $R_2^1(6)$, (c) $R_4^2(8)$, (d) $R_6^4(16)$, (e) $R_4^4(12)$, $R_8^6(24)$ and (g) $R_4^4(n)$ motifs in salts derived from mono- and dicarboxylic acids.

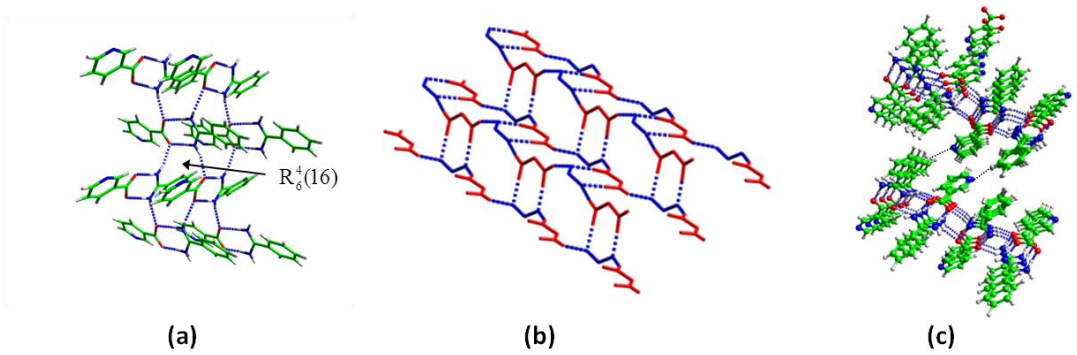

Figure 1. Hydrogen bonding motif in **1**. (a) 2D network with $R_2^2(8)$ and $R_6^4(16)$ motifs. (b) Side view showing the undulated sheet structure. For the sake of clarity, the aromatic rings of benzamidinium and nicotinate are not shown. Amidine groups in red, carboxylate groups in blue. (c) C-H···N hydrogen bonding between neighbouring sheets.

As in **1**, pairs of hydrogen bonds between the benzamidinium group and the carboxylate group of salicylic acid give rise to the $R_2^2(8)$ synthon which builds up infinite ribbons in $bzamH^+sal^-$ (**2**, Figure 2). H bonding interactions between the amidinium group and the carboxylate group of the adjacent ion pair generate $R_4^2(8)$ rings. The phenol group of salicylate acts as an intramolecular H bond donor to the carboxylate group and accepts an N-H hydrogen bond from the next $bzamH^+\cdots sal^-$ unit. The latter interaction results in 12-membered rings ($R_4^4(12)$). Ribbons of $bzamH^+\cdots sal^-$ pairs are stacked along the *a* axis. In contrast to **1**, there are no interactions between adjacent stacks in **2**.

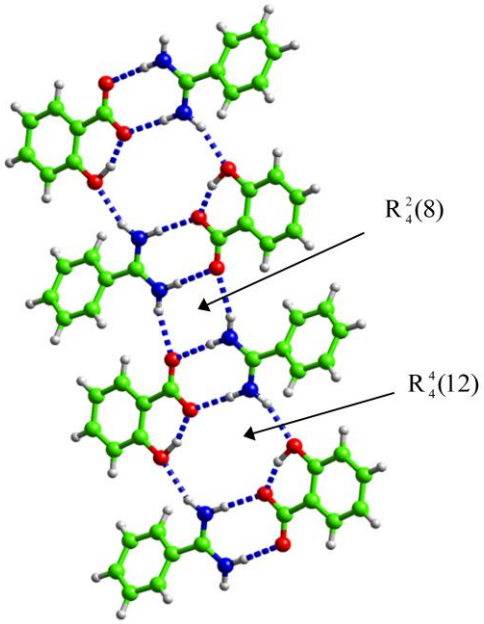

Figure 2. Hydrogen bonding motif in **2**. Ribbons of hydrogen bonded $bzamH^+\cdots sal^-$ ion pairs run along the *b* direction.

Figure 3 shows the 2D array of $R_2^2(8)$, $R_4^2(8)$ and $R_8^6(24)$ ring motifs observed in bzamH$^+$pab$^-$ (**3**). Similar to **1**, hydrogen bonding interactions between the benzamidinium and carboxylate groups give rise to an undulated sheet structure that is stabilized by stacking interactions between adjacent aromatic rings. There are two crystallographically independent bzamH$^+$pab$^-$ ion pairs per unit cell building up crystallographically independent sheets that are linked through H bonding interactions between the *p*-amino groups. (Figure 3c). The amino groups of sheet A act as H bond donors, while those of sheet B serve as H bond acceptors.

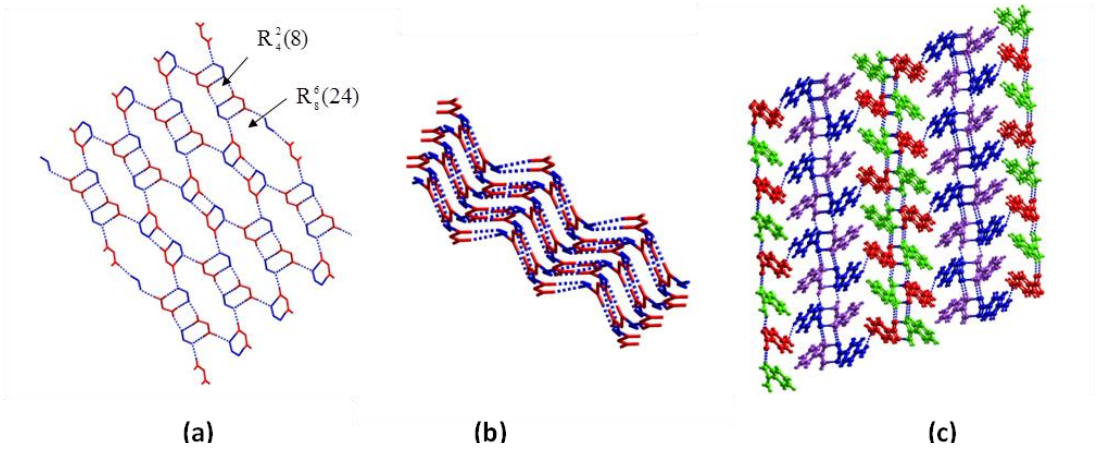

Figure 3. Hydrogen bonding motif in **3**. (a) 2D network with $R_2^2(8)$, $R_4^2(8)$ and $R_8^6(24)$ motifs. Amidine groups in red, carboxylate groups in blue. (b) Side view showing the undulated sheet structure. For the sake of clarity, the aromatic rings of benzamidinium and *p*-aminobenzoate are not shown. (c) Stacking interactions within sheets and hydrogen bonding between the amino groups of neighbouring sheets.

Slow evaporation of a 1:1 mixture of benzamidine and the dicarboxylic acid malonic acid in methanol gave bzamH$^+$malo$^-$ (**4**) consisting of a benzamidinium cation and a hydrogen malonate anion. The X-ray structure of **4** is depicted in Figure 4. The structural parameters are in line with the presence of the mono anion. For one of the carboxyl groups there is a clearly distinct 0.087 Å C-O bond length difference with C-O and C=O bond lengths of 1.298(2) and 1.211(2) Å respectively whereas the other carboxyl group has a C-O bond length difference of just 0.036 Å. Generally, a difference of ≤ 0.03 Å is indicative of a deprotonated carboxylate group, while in a protonated carboxyl group the C-O bonds differ by ≥ 0.08 Å.[32] The hydrogen malonate anion is known to adopt different conformations and H bonding schemes

in its salts. In the sodium,[33] ammonium[34] and methylammonium[35] salts, hydrogen malonate ions are linked into chains by short intermolecular H bonds with the two carboxyl groups being nearly perpendicular to each other. H bonded chains of hydrogen malonate anions are also present in the potassium salt, however, the two carboxyl groups are co-planar.[36] By contrast, an extremely short asymmetric intramolecular H bond (graph-set notation S(6); Speakman's type B) is observed in guanidinium,[37] benzylammonium, 4-picolinium,[38] melaninium hydrogen malonate,[39] and in partially deuterated sodium trihydrogendimalonate with a nearly planar conformation of the monoanion.[40] In trimethoprim hydrogen malonate the carboxyl and carboxylate groups form an intramolecular H bond and the dihedral angle is 18.8(2)º. As in the guanidium salt, the hydrogen malonate anion in **4** is stabilized by a short intramolecular H bond of Speakman's B_2 type.[41] The O···O distance of 2.422(2) Å is at the low end of the range observed in other salts (2.41 – 2.51 Å[37-40]), while the O-H···O angle is less bent (161 º in **4**, typical range 153-159 º [37-40]). The carboxyl and carboxylate groups form a dihedral angle of 5.6(5) º. The deprotonated carboxyl group (O1, O2) forms a pair of H bonds with the amidinium group to give the $R_2^2(8)$ synthon. In addition, O1 accepts a second H bond from N2 of the neighbouring $bzamH^+\cdots malo^-$ pair resulting in an $R_4^2(8)$ ring. Furthermore, hydrogen bonding interactions between N1 and the carbonyl oxygen of the protonated carboxyl group generate 16-membered rings ($R_4^4(16)$, Scheme 1g). Overall, the charge-assisted N-H···O hydrogen bonds in **4** give rise to a ribbon-type structure. In the crystal packing, ribbons stack along the body diagonal of the unit cell. There are no hydrogen bonds between neighboring tapes.

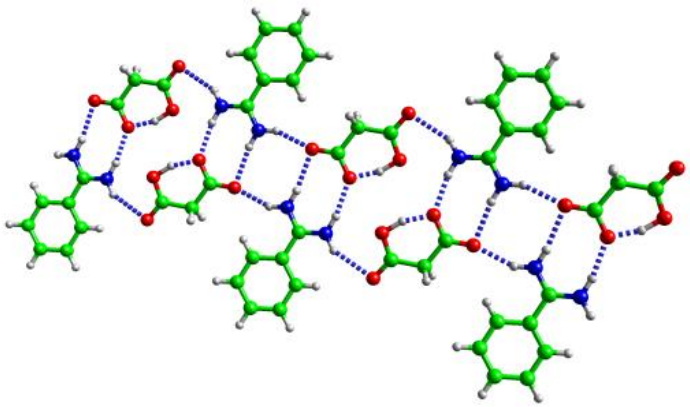

Figure 4. Hydrogen bonding motif in **4**.

The hydrogen maleate salt bzamH$^+$male$^-$ (**5a**) was crystallized from methanol, ethanol and water. There are three crystallographically independent cations, designated A, B, and C and three crystallographically independent anions, designated a, b, and c, in the asymmetric unit (Figure 5). The hydrogen maleate anions feature the strong intramolecular H bond (O···O 2.434(2) - 2.442(2) Å; ∠(O-H···O) 173(2) - 176(2) º) typically found in the mono anion of maleic acid. H bonding interactions between cations and anions lead to a tape-like structure. The bzamH$^+$ cations A and B are linked *via* pairs of H bonds to the hydrogen maleate anions a and b ($R_2^2(8)$). The third bzamH$^+$ cation (C) and anion c form an $R_2^1(6)$ motif with both NH_2 groups interacting with one of the carbonyl oxygens. The A:::a and B:::b ion pairs are connected through N···O H bonds giving rise to eight-membered rings ($R_4^2(8)$). The other nitrogen of B donates a hydrogen bond to the protonated carboxyl group of a neighbouring B:::b pair so that two B:::b pairs form an 16-membered ring ($R_4^4(16)$, Scheme 1g). The carbonyl oxygens of the protonated carboxyl groups of a and c act as H bond acceptors to an amidine nitrogen of A and C, respectively, so that H bonding interactions between neighbouring C:::c and A:::a pairs generate $R_4^4(18)$ motifs. In addition $R_4^4(12)$ rings result from H bonding interactions between a carboxylate oxygen of c and a benzamidinium nitrogen of the next C:::c pair. Overall, the tape-like structure consists of a sequence of fused $R_4^4(16)$, $R_2^2(8)$, $R_4^2(8)$, $R_4^4(18)$, $R_2^1(6)$, and $R_4^4(12)$ rings.

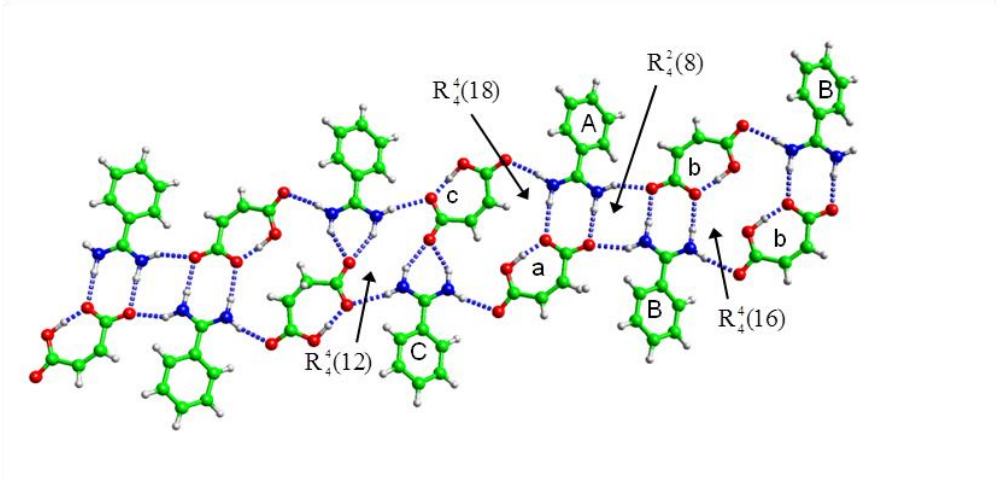

Figure 5. Hydrogen bonding motif in **5a**.

In contrast to malonic and maleic acid, pimelic acid forms a 2:1 salt with benzamidine. As shown in Figure 6, both carboxylate groups are involved in the $R_2^2(8)$ motif and accept an additional H bond from a neighbouring benzamidinium cation. The latter generates a 2D structure of $R_4^4(28)$ fused rings.

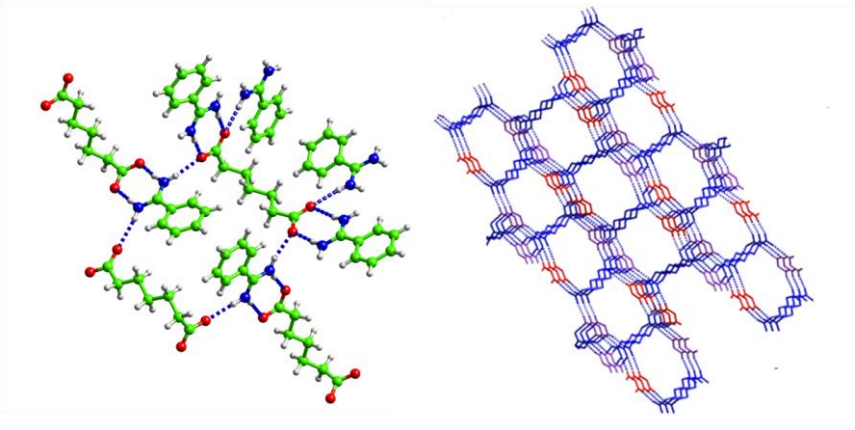

Figure 6. Hydrogen bonding motif in $(bzamH^+)_2pim^{2-}$ (**6**). Right: Aromatic rings and hydrogen atoms bonded to carbons are omitted for clarity. Benzamidine groups in red, pimelic acid in blue.

H Bonding Motifs in Benzamidinium Amidates and Sulfonamidates. The X-ray structures of the benzamidinium salts of the sulfonamides sulfathiazole (**7**) and sulfamerazine (**8**) are depicted in Figure 7. In both structures, cations and anions are paired through charge-assisted N-H···N hydrogen bonding interactions with the deprotonated sulfonamide nitrogen and a heterocyclic ring nitrogen acting as H bond acceptors ($R_2^2(8)$, Scheme 2). While the imido tautomer is dominant in the solid state structure of neutral stz with the proton residing on the heterocyclic nitrogen, the $C\text{-}N_{sulfonamidic}$ and $C\text{-}N_{ring}$ bond distances of 1.358(3) and 1.313(3) Å indicate that the sulfathiazole anion in **7** exists in the amido form with the sulfonamidic nitrogen retaining the negative charge. Likewise, the sulfamerazinate anion in **8** adopts the amidic form (as is the case in all known polymorphs of neutral smz[42-44]). The angles between the phenyl and the heterocyclic rings of the sulfonamidate in **7** and **8** are 81.96(9) º and 81.31(12) º in line with a gauche conformation when viewed along the S-N vector similar to the solid-state structures of stz and smz polymorphs. **7** features $R_4^4(12)$ rings in which two $bzamH^+$:::stz^- $R_2^2(8)$ pairs are connected *via* $O_{sulfonyl}\cdots N_{bzamH}$ hydrogen bonds.

In addition to the $R_2^2(8)$ motif in **8**, four smz anions are linked into 22-membered rings through H bonds between the amino substituent on the phenyl ring and the SO_2 group (Figure 7c). As both amino hydrogens and both sulfonyl oxygens participate in H bonding, a motif of fused $R_4^4(22)$ rings results. It should be noted that only one of the endocyclic nitrogens of the smz anion (the one para to the methyl group) acts as a H bond acceptor in **8**.

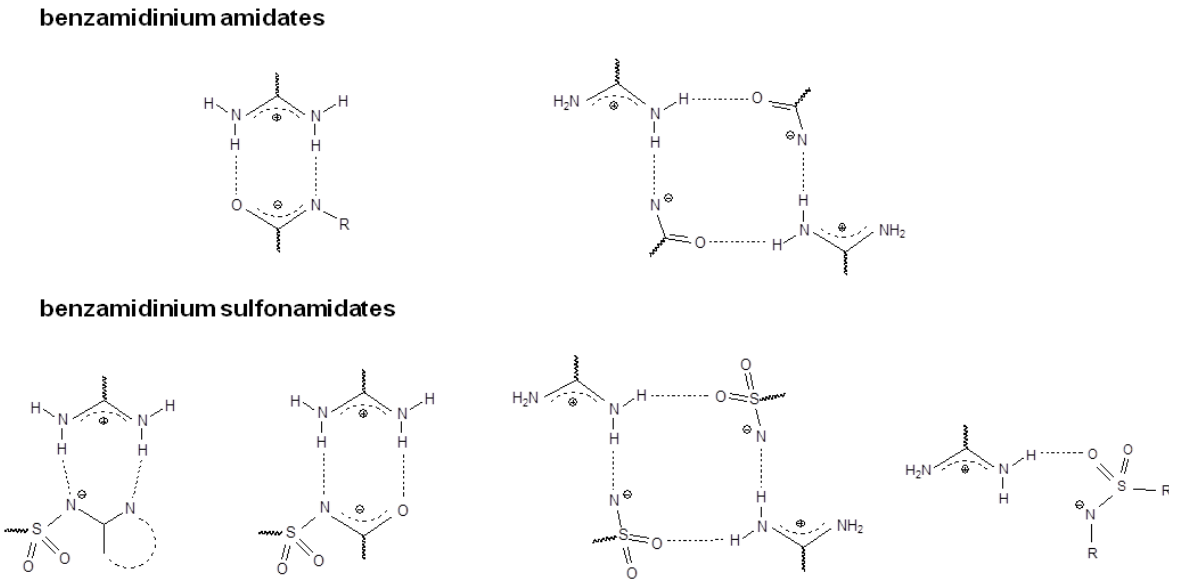

Scheme 2. $R_2^2(8)$ and $R_4^4(12)$ motifs and discrete hydrogen bonds in benzamidinium amidates and sulfonamidates.

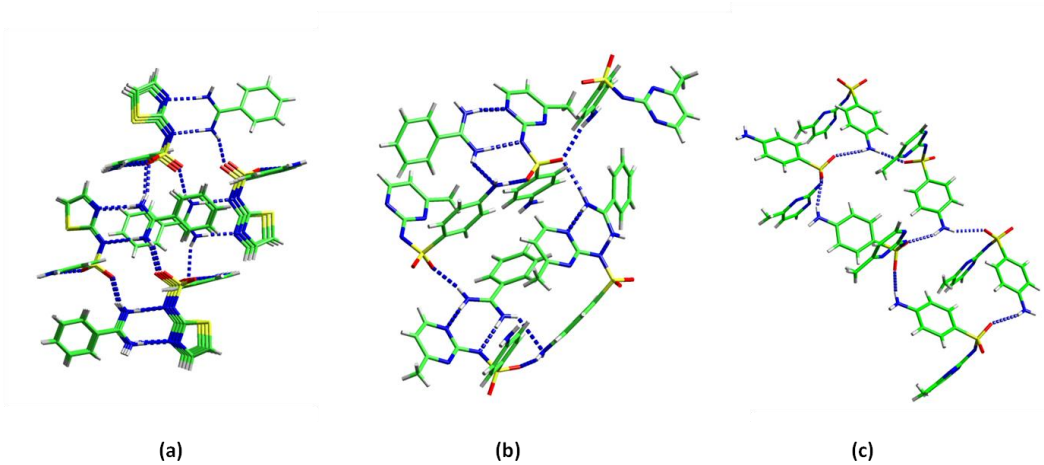

Figure 7. Hydrogen bonding motif in (a) $bzamH^+stz^-$ (**7**) and (b) $bzamH^+smz^-$ (**8**).
(c) $R_4^4(22)$ rings built up by smz anions in **8**.

Figure 8 shows the H bonding pattern in $bzamH^+sac^-$ (**9**). The usual ion pairs with $R_2^2(8)$ motif are generated through H bonding interactions of the benzamidinium group with the amide oxygen and the deprotonated amide nitrogen of saccharinate. Four $bzamH^+:::sac^-$ pairs build up 20-membered rings through $N_{bzamH}\cdots O_{sulfonyl}$ and $N_{bzamH}\cdots O_{amide}$ interactions ($R_6^5(20)$). In contrast to **7** and **8**, only one of the oxygens of the sulfonyl group of saccharinate is involved in H bonding.

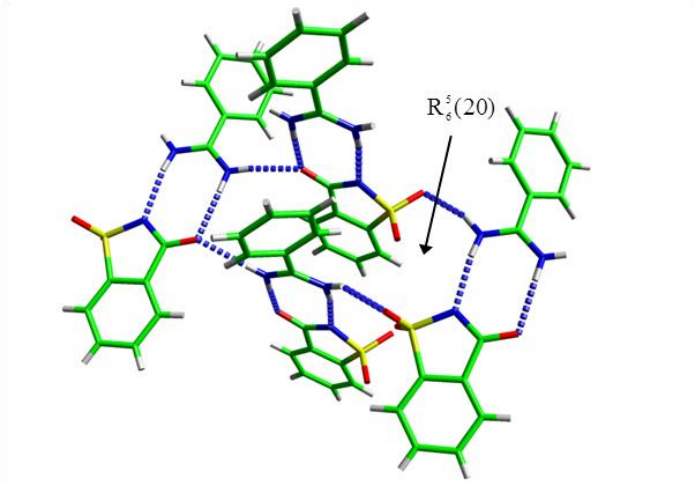

Figure 8. Hydrogen bonding motif in $bzamH^+sac^-$ (**9**).

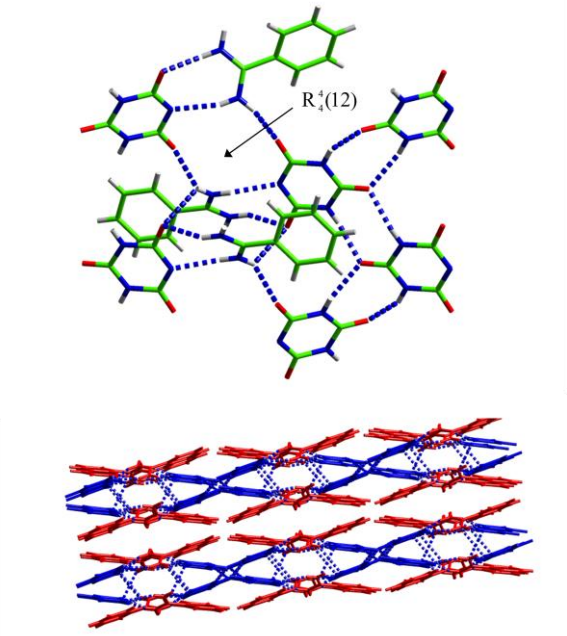

Figure 9. Hydrogen bonding motif (top) and double-layer structure (bottom) in $bzamH^+cya^-\cdot H_2O$ (**10**). The water molecules of crystallization have been omitted for clarity. Cyanurate anions in blue, benzamidinium cations in red.

The cyanurate salt of benzamidine crystallizes as the monohydrate bzamH^+cya$^-$·H_2O. The C-O bond lengths range from 1.231 to 1.238 Å indicating that the monoanion of cyanuric acid exists in the tri-keto tautomeric form. The cyanurate monoanions are connected through pairs of NH···O=C hydrogen bonds involving the two neutral (*N4,O3* and *N5,O3*) amide sites (non-planar $R_2^2(8)$ motif, Figure 9). Hydrogen bonding interactions of the benzamidinium group with the deprotonated (*N3,O1*) amide site result in the heteromeric $R_2^2(8)$ synthon. $R_2^2(8)$ heteromers associate through hydrogen bonding between an amidinium proton and O2, thus generating $R_4^4(12)$ rings leading to a double layer-type 2D structure (Figure 9). The water molecules of crystallization are situated between the double layers and hydrogen bond with the amidine nitrogens and amide O2 oxygens of neighbouring layers.

Among the larger rings that contain at least two cations and two anions, the most frequently found motifs in the benzamidinium salts studied here are centrosymmetric $R_4^2(8)$ and $R_4^4(n)$ rings with *n* most often being 12. However, these motifs are absent in **1** and **9** that both crystallize in the non-centrosymmetric space group $P2_1$. Instead, **1** and **9** are the only structures in which cations and anions assemble into non-centrosymmetric $R_6^4(16)$ (**1**) and $R_6^5(20)$ (**9**) rings. The third salt that crystallizes in a non-centrosymmetric space group is pimelate **6** (space group $P2_12_12_1$). The structure features $R_4^4(28)$ rings that are non-centrosymmetric because the two aryl rings of the two bzam cations lie on the same side of the ring plane.

Crystal Habits. Molecules or ionic compounds with crystal lattices with dominant intermolecular interactions in one direction often show anisotropic crystal growth and tend to give needle-like crystals. The control of anisotropic crystal growth and understanding the factors that affect crystal habit such as the choice of solvent and the presence of impurities or additives are of significant current interest, both in fundamental and applied research, as needle-shaped crystals are troublesome in industrial processes. Of the benzamidinium salts described in this paper **5a**, **6**, **8**, and **10** show pronounced anisotropic crystal growth. The face indexation of **6** which crystallizes as needles is shown in the Supporting Information. The needle direction, *i.e*. the direction of rapid growth is *a*. In the crystal packing, the benzamidinium cations and pimelate anions are stacked along this axis with an average of

42% of the atoms in van der Waals contact. The 2D H bonding network of fused $R_4^4(28)$ rings extends in the *bc* plane, with the pairs of H bonds of the heterodimers running parallel to *b*. Thus, the crystal growth of **6** is determined by conventional π stacking interactions rather than by hydrogen bonding. In **10**, the 2D network of $R_2^2(8)$ and $R_4^4(12)$ synthons extends parallel to the *ac* plane, while stacking interactions with a centroid···centroid distance of 3.59 Å between alternating benzamidinium cations and cyanurate anions are observed along the *b* axis. Again in this case the direction of rapid growth is along the stacking direction *b*. **8** contains a non-flat anion and the structure is not stacked. The heterodimers with $R_2^2(8)$ motif are linked *via* S=O···NH_2 H bonding interactions along the *b* axis and the needles extend in this direction (Supporting Information). The 2D network of the 22-membered rings built up by the anions is arranged parallel to the *ac* plane. This network is based on H bonding interactions between the sulfonyl oxygens and the amino substituent on the phenyl ring of sulfamerazinate (S=O···NH_2 2.993(4) and 3.048(5) Å). By contrast, one of the amino nitrogens of the positively charged benzamidinium group is involved in H bonding along *b* (S=O···NH_2 2.910(4) Å). The N···O distances reflect the greater strength of the charge-assisted interactions which determine crystal growth. It is a possible scenario that the heterodimers exist in solution and it can be speculated that a positively charged amino group on the crystal surface acts as a pivotal point for incoming dimers. **5a** grows into extremely large needles of up to > 3 cm length from aqueous solution (Figure 10). In the crystal structure, $bzamH^+$ cations of neighbouring $bzamH^+\cdots smz^-$ ribbons are stacked along the *a* direction with the centroid-centroid distance being 3.815 Å. The ribbons of fused $R_4^4(16)$, $R_2^2(8)$, $R_4^2(8)$, $R_4^4(18)$, $R_2^1(6)$, and $R_4^4(12)$ rings run perpendicular to the *ab* plane. Again, the needle growth is in the stacking direction (Supporting Information). Extended growth in the stacking direction of flat molecules such as benzoic acid, 1,4-naphthaquinone and β-phthalocyanine has been discussed in the literature.[45] It has been proposed that the formation of a new step in the stacking direction is a low energy process which will give growth in that direction a kinetic advantage. Our own recent study on the anisotropic crystal growth of flat and non-flat molecules with H bonding capacity has shown for 12 representative examples that extended needle growth is in the stacking direction, *i.e.* in the direction of the weaker interaction.[46] We have argued that a growth mechanism driven by dispersion forces should be

more effective for crystal growth than one driven by H bonding. Due to the short range of dispersion forces, molecules are less likely to be incorporated incorrectly.

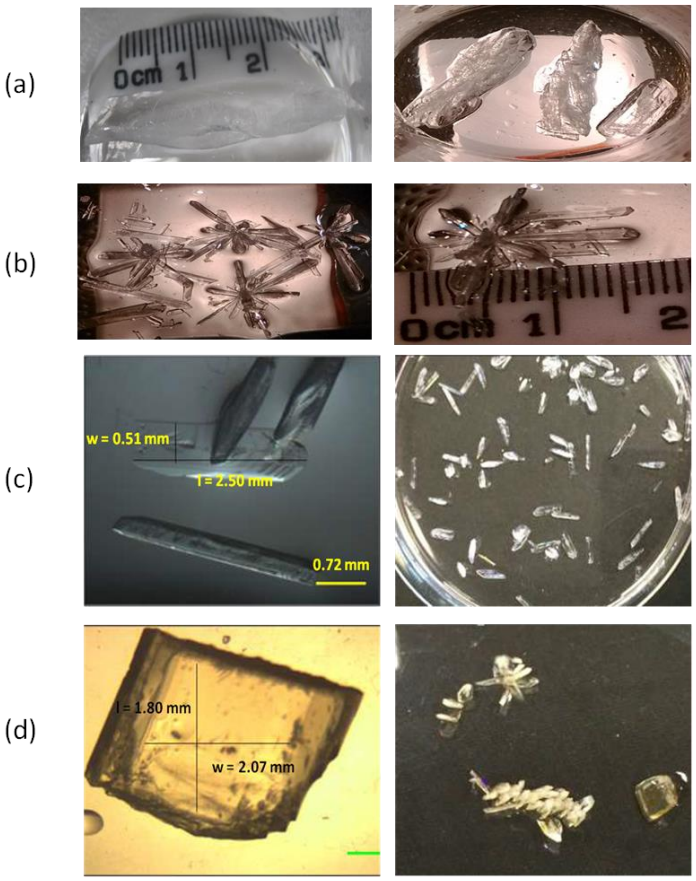

Figure 10. Crystals of benzH^+male$^-$ grown from (a) aqueous solution, (b) ethanol, (c) saline (0.03 M) and (d) ethanol in the presence of 5 mol% 2-picolylamine.

As **5a** shows the most extreme growth in the stacking direction, this salt was selected to study the effect of solvent and additives on crystal size and shape. **5a** was crystallized from ethanol, saline and from solutions containing heterocyclic additives that may interfere with crystal growth *via* π-π stacking with bzam. As evident from Figures 10b and c, both ethanol and saline gave a larger number of smaller and shorter needles. The XRPD patterns of the needles grown from ethanol and saline were identical to the simulated pattern of **5a**. The lower the polarity of the solvent, the stronger is the interaction between ion pairs in solution. Ethanol should favour the association of the heterodimers in solution leading to increased nucleation at the expense of crystal growth. By contrast, in aqueous solution crystal growth

prevails over nucleation as clearly seen in Figure 10a. The influence of inorganic salts on the growth of γ-glycine and DL-alanine crystals has recently been discussed in the literature.[47] Coulombic ion-surface interactions (which are stronger than solvent-surface interactions) can have two opposing effects: surface roughening (*i.e.* the generation of more kinks or defects) which promotes face growth and surface blocking which inhibits face growth by preventing solute molecules from integrating into the crystal lattice.[47-49] It has been proposed that the net effect of inorganic salt ions is determined by the strength of the ion-surface interaction with the crystal surface blocking effect outweighing the surface-roughening effect, when the interaction is very strong. In **5a** planar $bzamH^+\cdots male^-$ dimers are stacked in the needle growth direction. Two different scenarios are possible: (1) benzamidinium cations and maleate anions attach as dimers to the growing crystal face. There is no net positive or negative charge and interactions of the Na^+ and Cl^- ions with crystal faces are expected to be weak. Surface blocking leading to shorter needles could be caused by cation-π interactions, however, Figure 10c shows that the needles are also thinner compared to those obtained from water. This suggests the second scenario (2) in which the $bzamH^+$ cations and $male^-$ anions attach to the growing crystal surface independently from each other and interactions with the saline ions hinders growth in all directions.

When 5 mol% 2-pyridine-carbaldehyde or 2-picolylamine was added to the solution, large, cubic crystals formed alongside needle-like **5a** (Figure 10d). Cubes and needles were manually separated and a small plate was cut from one of the cubes for single-crystal strcture determination. X-ray analysis revealed that the cubic crystals were a second polymorph **(5b)** of $bzamH^+male^-$ (Figure 11). The asymmetric unit of **5b** comprises two crystallographically independent cations and two hydrogen maleate anions. Both hydrogen maleate anions feature one protonated carboxyl group (difference in C-O and C=O bond lengths > 0.08 Å) and one deprotonated carboxylate group with C-O bond lengths that are identical within the standard deviations. The typical short O-H···O hydrogen bond is observed in both maleate mono anions (O···O = 2.433(2) and 2.440(2) Å). In one of the hydrogen maleate anions the carboxyl proton is approximately centred between both oxygens while in the other one the hydrogen is located closer to O3 (Table S1). As in **5a**, the $R_2^2(8)$ motif is present as the

deprotonated carboxylate groups of both anions pair with the benzamidinium group. The carbonyl oxygen of the protonated carboxyl group of both anions interacts with the benzamidinium nitrogens which gives rise to 16-membered rings.

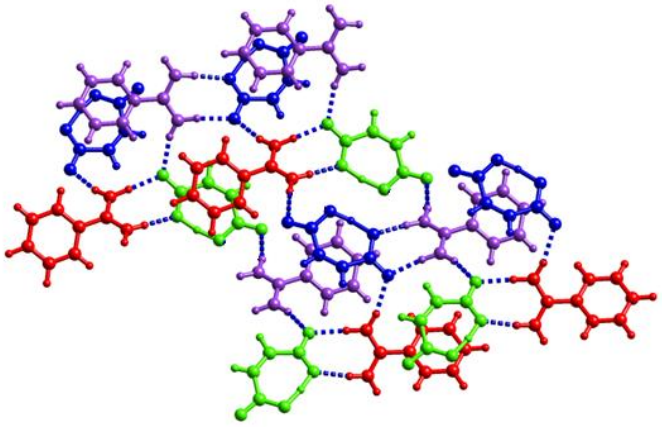

Figure 11. Hydrogen bonding motif in **5b**.

The structure of **5b** is that of a 3D hydrogen-bonded network and is not stacked. The cubic habit means that there is no preferred growth direction and this further supports the importance of stacking interactions in anisotropic crystal growth. In the absence of additives, only **5a** is observed, while **5a** and **5b** cocrystallize in the presence of 2-pyridin-carbaldehyde and 2-picolylamine. In the latter case it was also noted that **5a** grew more slowly and the needles had a smaller aspect ratio. This may be attributed to the aromatic additives interacting with the growing crystal surface through π-π interactions and hindering growth in the stacking direction, thus giving polymorph **5b** a kinetic advantage over **5a**.

Salt Formation *via* Solid-State and Liquid-Assisted Grinding. When bzam was ground with one equivalent of nicotinic acid, salicylic acid, *p*-aminobenzoic acid, sulfathiazole, saccharin or with 0.5 equivalents of pimelic acid using a mortar and pestle, the XRPD patterns of the ground mixtures were identical to the theoretical powder patterns generated from the single crystal data of **1**-**3**, **7**, **9** and **6** (Supporting Information). Grinding with malonic acid gave a hygroscopic, sticky material that could not be further analysed.

Neat grinding of an equimolar mixture of benzamidine and maleic acid gave polymorph **5b**. The same polymorph was obtained by liquid-assisted grinding with polar (ethanol, methanol) or non-polar (toluene) solvents. On grinding the isolated crystals of **5a** for 5 min. in the absence or presence of a drop of ethanol (using a mortar and pestle), a polymorphic transformation to **5b** was observed (Supporting Information). The formation and conversion of the two polymorphs of bzamH$^+$male$^-$ is summarised in Scheme 3.

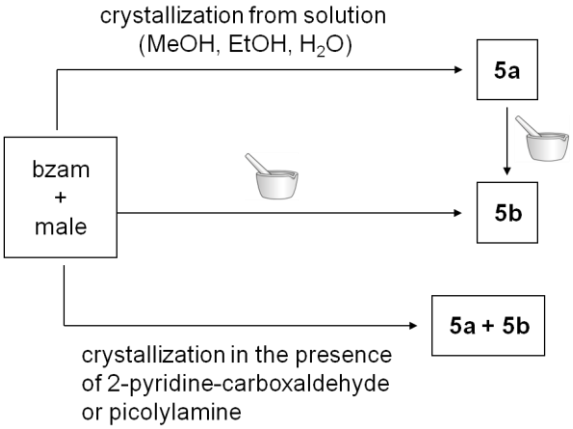

Scheme 3. Polymorphism of bzamH$^+$male$^-$.

The changes in the XRPD patterns of a stoichiometric mixture of smz and bzam upon grinding under different conditions are displayed in Figures S12 and S13. Smz has three known polymorphs; commercial form I (FI),[42] form II[43] which is the most stable polymorph at r.t. and form III which was discovered in 2006 and can be prepared in milligram quantities only.[44] The X-ray powder diffractogram recorded after grinding smz FI / bzam for 5 min. showed unchanged smz FI. Adding a drop of ethanol prior to grinding had no effect. However, the benzamidinium salt **8** was formed, when grinding was performed in a ball mill for 20 min. in the presence of substoichiometric amounts of ethanol (Figure S12). Interestingly, in the absence of any solvent, the XRPD pattern recorded after 20 min. ball-milling showed an amorphous halo (Figure S13). The diffractogram did not change, when the milling time was extended to 60 min. The solid remained X-ray amorphous, when kept at 25 % relative humidity (RH) for two weeks. A detailed study on the effect of ball-milling of smz

in the absence and presence of various carboxylic acids has been previously reported by us.[50] It was found that fully X-ray amorphous smz can only be obtained by cryo-milling, when the low temperature prevents re-crystallization during milling and that even when stored under vacuum, crystallisation occurs within a few hours. Certain carboxylic acids were shown to stabilize the amorphous phase by forming a co-amorphous system with smz, while milling of smz FI at r.t. in the absence of additives resulted in the polymorphic transformation to FII. Co-amorphous systems are of interest for the formulation of BCS (Biopharmaceutical Classification System) class II and IV drugs due to the enhanced dissolution properties of the amorphous phase. In view of this it was of interest to distinguish whether the rapid amorphisation during r.t. milling and the higher stability of the amorphous 1:1 smz/bzam mixture compared to amorphous smz alone were due to the formation of the amorphous salt or a co-amorphous system. The most prominent band in the IR spectrum of smz is the sharp, strong band of the symmetric stretching vibration of the sulfonyl group at 1150 cm^{-1}. This band is shifted to 1122 cm^{-1} in the spectrum of the amorphous solid. A shift of this magnitude is likely due to the deprotonation of the sulfonamide group rather than to a change in hydrogen bonding interactions as would be the case in a co-amorphous system. When the amorphous bzam/smz was stored at 72 % RH, crystallisation occurred within 24 h. The XRPD pattern, however, is different from that of the simulated pattern of **8** (Figures S12 and S13). On the other hand, the IR spectra of **8** and of the recrystallized sample are very similar. Again, the ν_{sy}(S=O) band is shifted to a lower wavenumber (1117 cm^{-1}) consistent with the presence of a deprotonated sulfonamide group. This led us to the conclusion that the recrystallized sample is another polymorph of **8** (**8a**) and that co-milling of bzam with smz generates an amorphous salt rather than a co-amorphous solid. Given the 4.5 pH units difference in pK_a value, salt formation between bzam and smz can be predicted, but would be expected to be more difficult under solvent-free conditions than the formation of a co-amorphous system due to the charge separation associated with the proton transfer (see below). It is noteworthy that dry-milling **8** also leads to amorphisation (Scheme 4).

The DSC plot of the amorphous phase obtained by ball-milling a 1:1 mixture of bzam and smz features two exotherms at 97.5 and 117.8 °, when a heating rate of 10 degrees/min is applied (Figure S14). The occurrence of two distinct crystallization exotherms in the DSC

traces of cryomilled organic glasses has been discussed in the literature. Different mechanistic models for bimodal crystallization (when the crystallization into different polymorphs or a polymorphic transformation can be excluded) have been suggested. Some authors propose the milling-induced formation of a defective crystalline state as a phase thermodynamically distinct from the true amorphous glass,[51,52] while others explain the two-peak crystallization event by a surface crystallization model involving faster surface crystallization due to the higher surface mobility followed by crystallization of bulk glass at higher temperature.[53,54] Chattoraj *et al*. have studied the crystallization behaviour of ten organic glasses prepared by cryomilling and shown that bimodal crystallization is observed when the crystallization onset (T_c) is below or near the glass transition temperature (T_g), whereas the crystallization event is unimodal, when T_c is well above T_g.[54] As evident from Figure S14 we do not observe a T_g in the standard DSC traces which is not surprising, as it would be buried by the first crystallization exotherm. When the heating rate is increased form 10 degrees/min to 30 degrees/min, the first crystallization exotherm shifts from 97.5 to 104.1 °C (Figure S14). Furthermore, the peak area of the first exotherm decreases while that of the second one increases. This behaviour is in line with the surface crystallization model. The slower the heating rate, the lower the temperature of the crystallization onset. At a slower heating rate more time is available for the surface to crystallize completely.[54] In addition to the two well-resolved exotherms, a small, broad exotherm appears at 176.1 °C which may be due to a polymorphic transformation. When a sample of **8a** is heated to 130 °C, a slow conversion to **8** takes place with diffraction peaks of **8** appearing after 30 min (Figure S15).

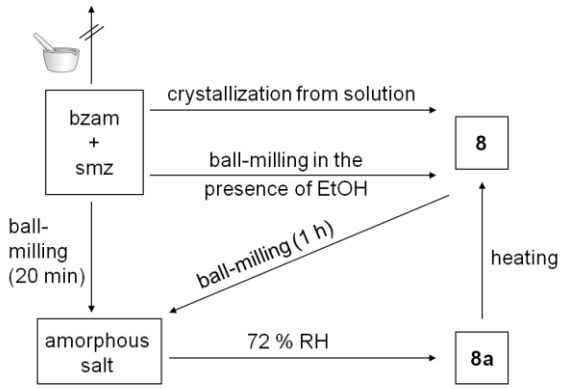

Scheme 4. Polymorphism of $bzamH^+smz^-$.

Ball-milling of bzam with cyanuric acid gave **10**. The underlying amorphous halos in the time-dependent XRPD patterns (Figure 12) suggest that the conversion takes place *via* the amorphous phase. A qualitative analysis of the XRPD patterns indicates that the percentage of amorphous content in the bzam/cya system reaches a maximum after 10 min. milling time. A similar observation has been made by us in the case of the mechanochemical synthesis of benzyladeninium maleate and sulfathiazolium oxalate.[55,56] During milling of benzyladenine/maleic acid and sulfathiazole/oxalic acid, both systems went amorphous before the diffraction peaks of the respective salt appeared in the XRPD patterns. Cyanuric acid has a melting point of > 300 °C. We have previously pointed out the difficulty of the mechanochemical salt formation of high melting acids under anhydrous or solvent-free conditions.[56]

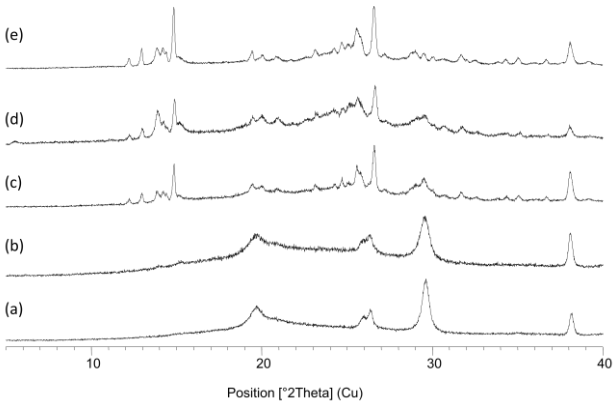

Figure 12. XRPD patterns of bzam/cya after ball-milling for (a) 5 min. (b) 10 min. (c) 15 min. (d) 20 min. and (e) 1 h.

Conclusions

A plethora of benzamidinium salts with supramolecular, H bonded network structures were obtained by mechanochemical synthesis and solution crystallization. In two cases, polymorphism was observed. The mechanochemical formation of $bzamH^{+}cya^{-}$ involves a transient amorphous phase. The solvent and the presence of an inorganic salt have a

pronounced effect on the crystal size of bzamH$^+$male$^-$. Depending on the crystallization conditions the average length of bzamH$^+$male$^-$ needles can vary between 0.25 and > 3 cm.

Supporting Information

Crystallographic information files. Details on H bonding interactions in 1 - **10**. Crystal images showing reciprocal axes and face normals and packing diagrams of **6**, **10**, **8** and **5a**. XRPD patterns of **1**- **6** and **9** prepared by grinding and theoretical patterns generated from single-crystal data. Comparison of the XRPD patterns of SMZ FI, FII, FIII, **8** and after manually grinding and solvent-drop ball milling a stoichiometric mixture of smz FI and bzam. Comparison of the XRPD patterns of SMZ FI, FII, FIII, after 20 min. ball-milling of a stoichiometric mixture of bzam and smz and after storage of the ball-milled bzam/smz mixture for 1 d at 72 % relative humidity. DSC plots of amorphous bzamH$^+$smz$^-$ at different heating rates. XRPD patterns of **8a** after heating for different time intervals. This material is available free of charge via the Internet at http://pubs.acs.org.

Acknowledgements

This work was supported by Science Foundation Ireland under Grant No. [07/SRC/B1158] as part of the Synthesis and Solid State Pharmaceutical Centre (SSPC). Mr. Dermot McGrath is thanked for DSC measurements.

References

(1) Perrine, D.; Chenu, J. P.; Georges, P.; Lancelot, J. C.; Saturnino, C.; Robba, M. *Antimicrob. Agents Chemother.* **1995**, *39*, 339–342.

(2) Nguewa, P. A.; Fuertes, M. A.; Cepeda, V.; Iborra, S.; Carrión, J.; Valladares, B.; Alonso, C.; Pérez, J. M. *Chem. Biodivers.* **2005**, *2*, 1387–1400.

(3) Nehrbass-Stuedli, A.; Boykin, D.; Tidwell, R. R.; Brun, R. *Antimicrob. Agents Chemother.* **2011**, *55*, 3439–3445.

(4) Pegg, A. E. *Biochem. J.* **1986**, *234*, 249–262.

(5) Pegg, A. E. *Cancer. Res*. **1988**, *48*, 759–774.

(6) Smith, R. A.; Kirkpatrick, W. (eds.) "Ribavirin: structure and antiviral activity relationships". *Ribavirin: A Broad Spectrum Antiviral Agent*. New York: Academic Press., 1980, pp. 1–21.

(7) Soeiro, M.; de Souza, E. M.; Boykin, D. W. *Expert Opin. Ther. Patents* **2007**, *17*, 927–939.

(8) Venturini, G.; Menegatti, E.; Ascenzi, P. *Biochem. Biophys. Res. Commun*. **1997**, *232*, 88–90.

(9) Markwardt, F.; Landmann, H.; Walsman, P. *Eur. J. Biochem*. **1968**, *6*, 502–506.

(10) Markwardt, F.; Walsmann, P. *Experientia*, **1968**, *24*, 25–26.

(11) Babatunde, O.; Dunbar, P. G.; Durant, G. J.; Nagy, P. I.; Huzl III, J. J.; Periyasamy, S.; Ngur, D. O.; El-Assadi, A. A.; Hoss, W. P.; Messer, W. S. Jr *Bioorg. Med. Chem*. **1996**, *4*, 1605–1615.

(12) Heck, M. P.; Vincent, S. P.; Murray, B. W.; Bellamy, F.; Wong, C.-H.; Mioskowski, C. *J. Am. Chem. Soc*. **2004**, *126*, 1971–1979.

(12) Tong, M. K.; Papandreou, G.; Ganem, B. *J. Am. Chem. Soc*. **1990**, *112*, 6137–6139.

(14) Ganem, B.; Papandreou, G. *J. Am. Chem. Soc*. **1991**, *113*, 8984–8985.

(15) Papandreou, G.; Tong, M. K.; Ganem, B. *J. Am. Chem. Soc*. **1993**, *115*, 11682–11690.

(16) Pan, Y. T.; Kaushal, G. P.; Papandreou, G.; Ganem, B.; Elbein, A. *J. Biol. Chem*. **1992**, *267*, 8313–8318.

(17) Blériot, Y.; Genre-Grandpierre, A.; Tellier, C. *Tetrahedron Lett*. **1994**, *35*, 1867–1870.

(18) Blériot, Y.; Dintinger, T.; Genre-Grandpierre, A.; Pradines, M.; Tellier, C. *Bioorg. Med. Chem. Lett*. **1995**, *5*, 2655–2660.

(19) Therisol, H.; Letourneux, Y.; Therisod, M. *Bioorg. Med. Chem. Lett*. **1998**, *8*, 371–372.

(20) Blériot, Y.; Dintinger, T.; Guillo, N.; Tellier C. *Tetrahedron Lett*. **1995**, *36*, 5175–5176.

(21) Guo, W.; Hiratake, J.; Ogawa, K.; Yamamoto, M.; Ma, S.-J.; Sakata, K. *Bioorg. Med. Chem. Lett*. **2001**, *11*, 467–470.

(22) Knapp, S.; Purandare, A.; Rupitz, K.; Withers, S. G. *J. Am. Chem. Soc*. **1994**, *116*, 7461–7462.

(23) Knapp, S.; Choe, Y. H.; Reilly, E. *Tetrahedron Lett*. **1993**, *34*, 4443–4446.

(24) James, S. L.; Adams, C. J.; Bolm, C.; Braga, D.; Collier, P.; Friscic, T.; Grepioni, F.; Harris, K. D. M.; Hyett, G.; Jones, W.; Krebs, A.; Mack, J.; Maini, L.; Orpen, A. G.; Parkin, I. P.; Shearouse, W. C.; Steed, J. W.; Waddell, D. C. *Chem. Soc. Rev*. **2012**, *41*, 413–447.

(25) Hasa, D.; Perissutti, B.; Cepek, C.; Bhardwaj, S.; Carlino, E.; Grassi, M.; Invermizzi, S.; Voinovich, D. *Mol. Pharmaceutics* **2013**, *10*, 211–224.

(26) Andre, V.; Braga, D.; Grepioni, F.; Duarte, M. T. Cryst. *Growth Des*. **2009**, *9*, 5108–5116.

(27) Trask, A. V.; Hayes, D. A.; Motherwell, W. D. S.; Jones, W. *Chem. Comm*. **2006**, 51–53.

(28) McArdle, P.; Gilligan, K.; Cunningham, D.; Dark, R.; Mahon, M. *CrystEngComm.* **2004**, *6*, 303–309.

(29) CrysAlisPro, Oxford Diffraction Ltd., Version 1.171.33.31 (release 08-01-2009 CrysAlis171.NET).

(30) SHELXT - Sheldrick, G. M. *Acta Crystallogr*. **2015**, *A71*, 3-8.

(31) SHELXL - Sheldrick, G. M. *Acta Crystallogr*. **2015**, *C71*, 3-8.

(32) Childs, S. L.; Stahly, G. P.; Park, A. *Mol. Pharmaceutics* **2007**, *4*, 323–338.

(33) Rao, S. N.; Parthasarathy, R. J. *Chem. Soc. Perkin Trans*. *2*, **1974**, 683–685.

(34) Chapuis, G.; Zalkin, A.; Templeton, D. H. J. *Chem. Phys*. **1975**, *62*, 4919–4922.

(35) Djinovic, K.; Golic, L. *Acta Cryst*. **1991**, *C47*, 2367–2371.

(36) Sime, J. S.; Speakman, J. C.; Parthasarathy, R. *J. Chem. Soc. A* **1970**, 1919–1923.

(37) Djinovic, K.; Golic, L.; Hadzi, L.; Orel, B. *Croat. Chem. Acta*, **1988**, *61*, 405–412.

(38) Djinovic, K.; Golic, L.; Leban, I. *Acta Cryst*. **1990**, *C46*, 281–286.

(39) Froschauer, B.; Weil, M. *Acta Cryst*. **2012**, *E68*, o2553–o2554.

(40) Kalsbeek, N. *Acta Cryst*. **1992**, *C48*, 878–883.

(41) Speakman, J. S. *Struct. Bonding (Berlin)*, **1972**, *12*, 141–199.

(42) Acharya, K. R.; Kuchela, K. N.; Kartha, G. *J. Crystallogr. Spectrosc. Res.* **1982**, *12*, 369–376.

(43) Caira, M. R.; Mohamed, R. *Acta Cryst*. **1992**, *B48*, 492–508.

(44) Hossain, G. M. G. *Acta Crystallogr Sect E Struct Rep Online* **2006**, *62*, o2166–o2167.

(45) Panina, N.; van de Ven, R.; Janssen, F. F. B. J.; Meekes, H.; Vlieg, E.; Deroover, G. *Cryst. Growth Des.* **2008,** *9*, 840–847.

(46) Walshe, N.; Crushell, M.; Karpinska, J.; Erxleben, A.; McArdle, P. *Cryst. Growth Des*. **2015**, *15*, 3235-3248.

(47) Han, G.; Chow, P. S.; Tan, R. B. H. *Cryst. Growth Des*. **2015**, *15*, 1082–1088.

(48) Shimon, L. J. W.; Addadi, M.; Vaida, L.; Lahav, M.; Leiserowitz, L. *J. Am. Chem. Soc*. **1990**, *112*, 6215–6220.

(49) Boume, J. R.; Davey, R. J. *J. Cryst. Growth* **1976**, *36*, 278–286.

(50) MacFhionnghaile, P.; Hu, Y.; Gniado, K.; Curran, S.; McArdle, P.; Erxleben, A. *J. Pharm. Sci*. **2014**, *103*, 1766–1778.

(51) Feng, T.; Pinal R.; Carajal, M. T. *J. Pharm. Sci*. **2008**, *97*, 3207–3221.

(52) Chamarthy, S. P.; Pinal, R. *Colloid Surface A* **2008**, *331*, 68–75.

(53) Trasi, N. S.; Boerrigter, S. X. M.; Byrn, S. R. *Pharm. Res*. **2010**, *27*, 1377–1389.

(54) Chattoraj, S.; Bhugra, C.; Telang, C.; Zhong, L.; Wang, Z.; Sun, C. C. *Pharm. Res*. **2012**, *29*, 1020–1032.

(55) McHugh, C.; Erxleben, A. *Cryst. Growth Des*. **2011**, *11*, 5096−5104.

(56) Hu, Y; Gniado,K.; Erxleben, A.; McArdle, P. *Cryst. Growth Des*. **2014**, *14*, 803-813.

For Table of Contents Use Only

Hydrogen Bonding Networks and Solid-state Conversions in Benzamidinium Salts

Naghmeh Kamali, Marwah Aljohani, Patrick McArdle* and Andrea Erxleben*

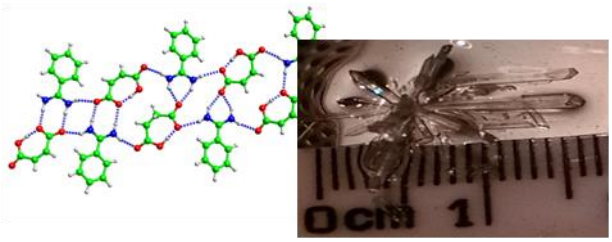

Ten benzamidinium salts with supramolecular, H bonded network structures were obtained by mechanochemical synthesis and solution crystallization. While several of the benzamidinium salts crystallize as needles, benzamidinium maleate grows into extremely large needles of up to >3 cm length from aqueous solution. The needle growth and the effect of the crystallization conditions on crystal size and shape are discussed.